Approved for public release; distribution is unlimited.

# An Infrared Focal Plane Array Camera System for Stereo-based Radiometric Imaging

January 1999

Douglas R. DeVoe
Shawn Goodrich
Russell Bauldree
James VanAnda

DeVoe & Matthews
Fort Walton Beach, FL 32548

## ABSTRACT

Results describe the development of a 3-5 micron infrared sensor sponsored by the Electro-Optical (EO)/Infrared (IR) Seeker/Sensor Systems Flight at the 46th Test Wing (TW/TSWI), Eglin AFB, Florida. The program is currently in Phase II with delivery of the prototype system in July, 1999. System design details and performance are presented. Results describe analytical derivations used in radiometric calibration along with a stereo-based photogrammetric technique used to estimate spatial position.

## 1.0 INTRODUCTION

The Electro-Optical (EO)/Infrared (IR) Seeker/Sensor Systems Flight at the 46 TW/TSWI Eglin Air Force Base, FL provides sensors, platforms and technical expertise to collect EO/IR signature measurements. Signature measurements are often for the Test and Evaluation (T&E) of new weapons systems and IR model development. Operating environments range from sub-tropical at Eglin Air Force Base, to desert conditions in Yuma, AZ, to an eastern European winter in Grayling, MI. Altitude varies from sea level to 50,000 feet. To date, new 2$^{nd}$ and 3$^{rd}$

# Form SF298 Citation Data

| **Report Date**<br>*("DD MON YYYY")*<br>00011999 | **Report Type**<br>N/A | **Dates Covered (from... to)**<br>*("DD MON YYYY")* |
|---|---|---|

| | |
|---|---|
| **Title and Subtitle**<br>An Infrared Focal Plane Array Camera System for Stereo-based Radiometric Imaging | **Contract or Grant Number** |
| | **Program Element Number** |
| **Authors** | **Project Number** |
| | **Task Number** |
| | **Work Unit Number** |
| **Performing Organization Name(s) and Address(es)**<br>DeVoe & Matthews Fort Walton Beach, FL 32548 | **Performing Organization Number(s)** |
| **Sponsoring/Monitoring Agency Name(s) and Address(es)** | **Monitoring Agency Acronym** |
| | **Monitoring Agency Report Number(s)** |
| **Distribution/Availability Statement**<br>Approved for public release, distribution unlimited | |
| **Supplementary Notes** | |
| **Abstract** | |
| **Subject Terms** | |
| **Document Classification**<br>unclassified | **Classification of SF298**<br>unclassified |
| **Classification of Abstract**<br>unclassified | **Limitation of Abstract**<br>unlimited |
| **Number of Pages**<br>17 | |

Generation Forward Looking IR (FLIR) systems and Advanced Imaging IR seekers are utilizing Focal Plane Array (FPA) technology. This technology presents great advances for IR imagery in sensitivity, frame rate, field-of-view (FOV) and instantaneous FOV (IFOV). New systems can look farther and sense targets that could not be detected five years ago.

A problem occurs when the T&E community is required to evaluate new weapon systems and aid in the development of accurate IR models for these new weapon systems. Calibrated measurement systems have not progressed to the levels of modern weapon systems and do not meet the IFOV requirements for model development. In addition, the requirement to collect these signatures at high speeds drives measurement groups to use mach-qualified turreted instrumentation pods, such as the 46 TW Supersonic Airborne Tri-Gimbaled Infrared System (SATIRS). The best systems for in-flight calibrated measurements are still the single detector scanning systems, because these systems are less susceptible to the thermal drift experienced with the dramatic temperature changes from sea level (20 °C) to altitudes of 40,000 ft (-40 °C). In addition, single detector systems are easier to calibrate and characterize. Scanning imagers also generally have better off-axis rejection than FPA imagers due to apertures and multiple reflections associated with scan mirrors. Scanning systems have IFOVs on the order of one mrad, whereas new FPA cameras have IFOVs on the order of 0.1 mrad. A measurement using a single detector system would result in an IFOV footprint of 10 feet, while the weapon system would have a footprint of one foot. The T&E community cannot effectively evaluate systems under these conditions. In addition, an FPA system can acquire several hundred frames per second, while a scanning system typically collects data at frame rates from six to 30 Hz. Extensive research of FPA systems in the early 1990's revealed serious problems with calibration and stability. By the mid-1990's, some progress had been made in stability; however, FPA systems still encountered calibration/drift problems when subjected to rigorous aircraft measurement environments. This technical shortfall resulted in the “Calibrated FPA Imager” Small Business Research Program (SBIR) in 1996. The Phase I specifications were:

1) 3 to 5 micron wavelength coverage
2) 0.1 mrad IFOV
3) 5 degree by 5 degree FOV
4) dynamic range of –20 °C to 1500 °C
5) range of operation: Sea Level to 50,000 foot Altitude.

The program is currently in Phase II with the delivery of the prototype in July, 1999. The remainder of this paper presents the technologies used to meet the defined shortfall.

## 2.0 SYSTEM DESIGN

The Focal Plane Array Calibrated System (FPACS) utilizes several features to help ensure radiometric accuracy. Some features help minimize unwanted radiation, while other aspects of the design provide an indication of a change in operating environment. Design features ensure radiometric accuracy where possible, and beyond that, the FPACS design ensures that the

operator is made aware when operating conditions may lead to radiometric inaccuracies. Primary components of FPACS are illustrated in Fig. 1. Components are 1) Optics, 2) FPA/Dewar, 3) Camera Electronics, 4) Pan & Tilt platform, and 4) Windows NT computer with a disk array storage system.

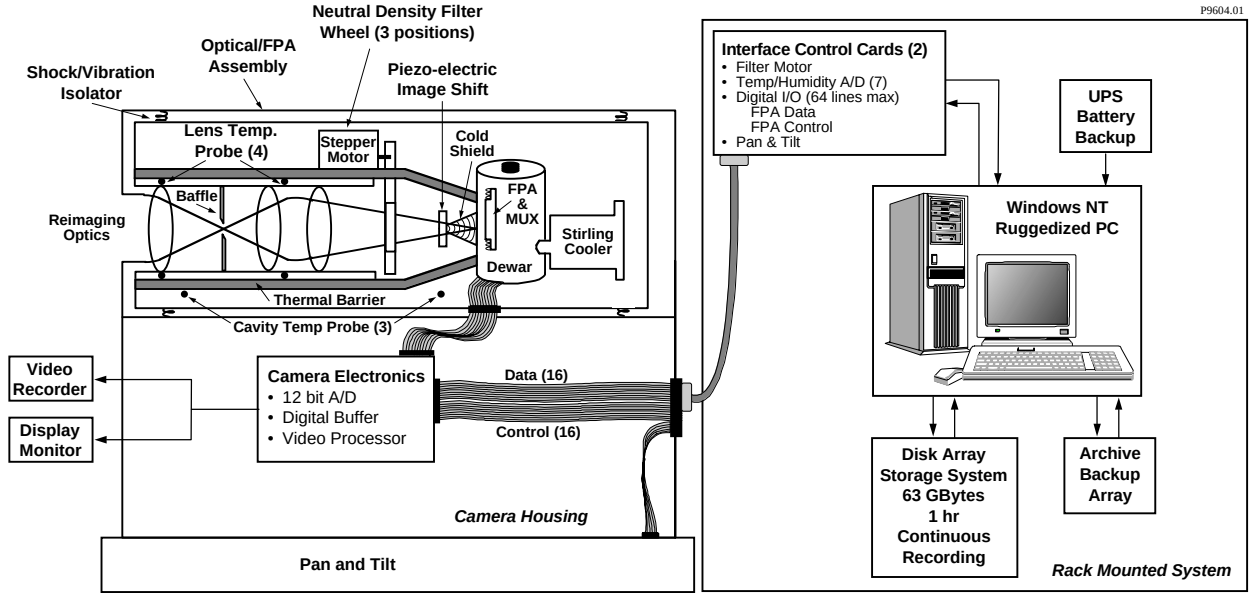

Figure 1. FPACS Block Diagram

## 2.1 OPTICAL DESIGN

The FPACS lens is an F/2, 180 mm focal-length lens consisting of twelve optical elements (Fig. 2). Lens material consists of a combination of Silicon, Germanium, and Zinc Selenide. An intermediate focal point with associated baffling is incorporated to help block stray radiation. In addition, a motorized, three-position filter wheel provides a clear aperture, a one percent transmisison filter, and an internal blackbody source. The transmission filter is used to help achieve the dynamic range requirement. The internal blackbody source provides an automated method of non-uniformity correction, and serves as a mechanism to assess radiometric stability. The blackbody source is designed to achieve the desired set point within a few seconds (-10 °C to 20 °C). The FPACS lens assembly also contains two internal temperature transducers that aid in monitoring overall radiometric stability.

A unique aspect of the system is a three millimeter germanium window mounted to a piezo-electric dithering device directly in front of the Dewar window. While not physically contained within the lens assembly, the germanium window is an active optical component that provides a one-half pixel shift of the image with respect to the focal plane. This image shift is a result of introducing a slight cant (horizontal or vertical) in the germanium window with respect to the plane of the Dewar window. The germanium's high index of refraction results in a translation large enough to enable over-sampling of the image. Optical resolution has been

correspondingly “over designed” to exploit this dithering mechanism. Figure 3 illustrates results from acceptance tests showing measurements of the optical blur circle with respect to the dimensions of a single pixel. For a static scene, dithering can be used to increase the effective resolution as well as compensate for isolated pixel outages. An example image acquired with the FPAC system is provided in Fig. 4. Image intensities have been modified to enhance overall scene detail. Individual mortar lines in the brick wall can be seen, as well as the barbed wire fence on the middle-left side of the image.

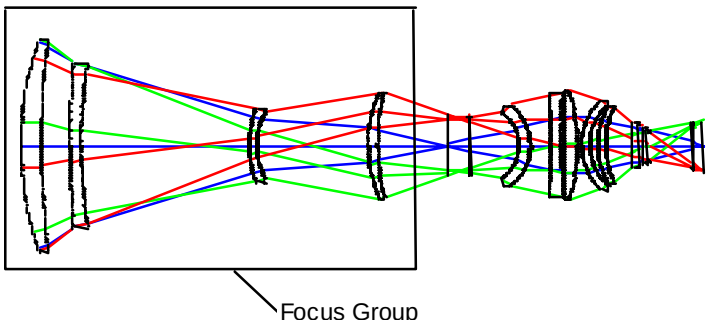


Figure 2. FPACS Lens Assembly

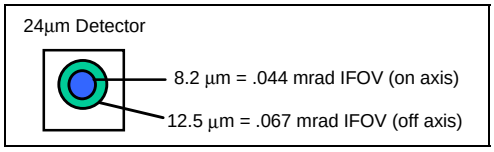


Figure 3. Spot Size (80% Energy)

Figure 4. FPACS Example Image

## 2.2 FPA/DEWAR

A photograph of the FPA/Dewar assembly and associated processing electronics is provided in Fig. 5. The dither device is in the foreground of the photo, shown mounted in front of the Dewar. The system incorporates a 512 pixel by 640 pixel Indium Antimonide (InSb) detector array. The detector array is cooled with a one Watt closed cycle Sterling cooler. The cooler and associated convection fins provide ample heat rejection capacity to help maintain a stable thermal environment within the camera enclosure.

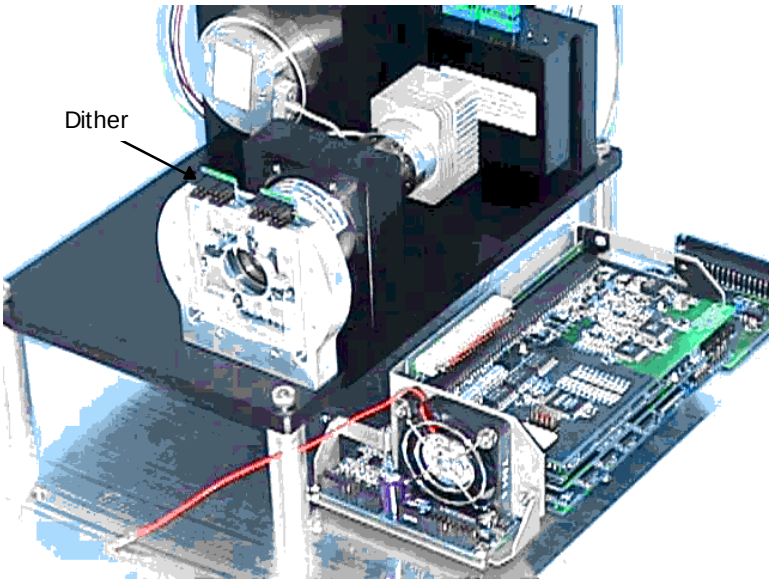


Figure 5. FPA/Dewar Assembly with Associated Processing Electronics

Unfortunately, not all detector elements in the array are usable. Some elements have essentially no response (so called “dead” pixels) while other detectors do not meet minimum performance criteria and are deemed inoperable. The amount and distribution of inoperable pixels is unique to each individual detector array. Selection of a suitable array depends on the application, availability, and budget. Manufacturers typically divide the array into regions, weighting the center region of the FPA more important than the outer edges. A large cluster of inoperable pixels near the center is less desirable, because the object being imaged is typically near the center. Inoperable pixels are not critical in applications where images are used for qualitative evaluation. In these applications, substitution of an inoperable pixel with the value from an adjacent pixel is an acceptable solution. However, pixel outages for a radiometric instrument are somewhat more problematic, particularly when outages are grouped together to form clusters. The dithering technique previously described provides an alternate method to recover missing values. Dithering is particularly advantageous, because missing values can be recovered from both vertical and horizontal directions. Figure 6 illustrates the distribution of inoperable pixels in the detector array used in the FPAC system. Inoperable pixels were empirically derived from an estimate of system response. Pixels exceeding two standard deviations from the mean response were deemed inoperable. Response was estimated from the change in pixel counts corresponding with a 2 °C change in calibration surface temperature. A ten pixel border along the left edge of the arrary has been omitted from the calculation, since this portion was not exposed to the calibration surface. In total, there are 46 pixel outages, four two-pixel cluster outages, two three-pixel outages, and 40 single pixel outages.

Indium Antimonide provides good thermal sensitivity in the 3-5 µm spectral region. Tests conducted by the manufacturer indicate an average Noise Equivalent Temperature Difference (NETD) of approximately 27 mK at 49 °C. This value is comparable with a system

NETD calculated from empirical data (Fig. 7). The procedure involved acquiring a sequence of 30 frames at 29 °C, 30 °C, and 31 °C then calculating the mean and standard deviation on a pixel-by-pixel-basis for each temperature. Data are "raw" detector values with no uniformity correction. The difference in temperature with respect to the difference between mean pixel counts was used to scale pixel count to degrees. This technique is employed as an approximation of the more rigorous solution described in Section 2.6. The standard deviation was calculated for each pixel at 30 °C and scaled to temperature. The resulting distribution is provided in Fig. 7. Results indicate a noise distribution slightly higher than manufacturer test results. In particular, data indicates a small portion of the image has a significantly higher than average noise level, as exhibitied by the right-hand "tail' in Fig. 7. Investigation into the distribution of these pixels revealed that this noise appears to be related to problems with individual rows. Work is in progress to correct this noise source. Even with the additional noise source, the average NETD is approximately 43 mK.

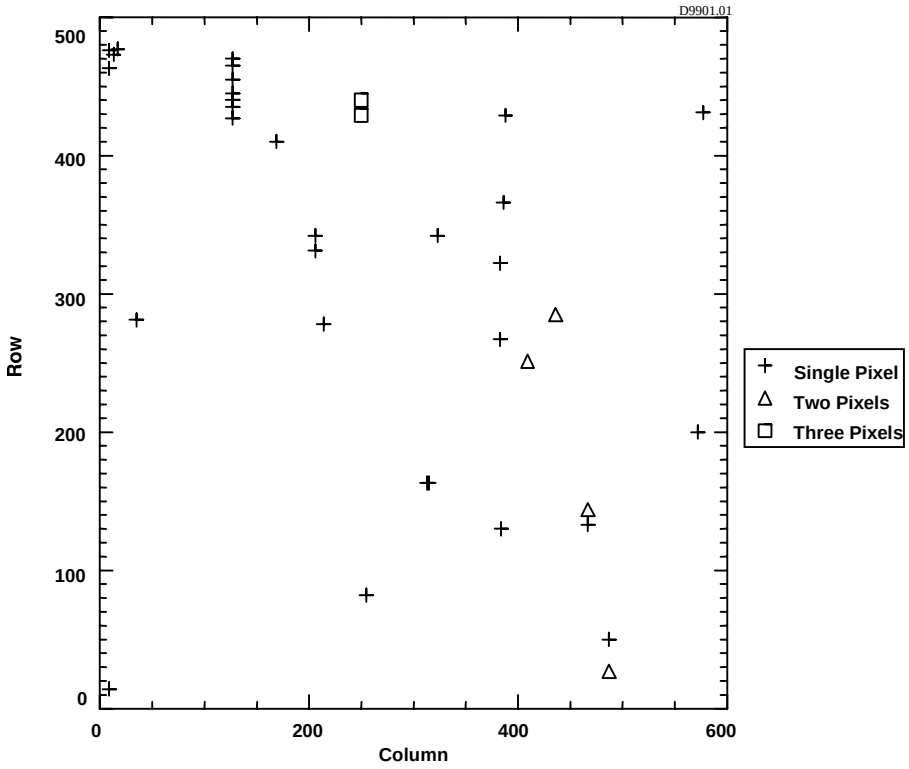


Figure 6. Inoperable Pixels in the 640 by 512 InSb FPA

Data used to calculate NETD also provides a technique to compare variations in system response. The mean count calculated for each pixel at 29 °C and 31 °C was divided by the two-degree temperature difference to provide a relative estimate of system response for each pixel. The distribution of pixel response in terms of counts per degree is shown in Fig. 8. Results show that deviations in response are large relative to noise deviations. The change in average pixel counts from 29 °C to 31 °C is approximately 102 counts. At 40 counts per degree, this change corresponds with a 2.6 °C change in temperature. At 60 counts per degree, the change in apparent temperature is 1.7 °C. Thus, for given change in counts, an uncorrected detector array could yield as much as a 0.9 °C difference in temperature estimate.

In addition to pixel response, another important aspect to be considered in establishing radiometric accuracy is offset correction. Figure 9 depicts the distribution of mean pixel values at 30 °C. The data demonstrates that bias correction is a significant aspect in establishing accurate estimates for an InSb FPA.

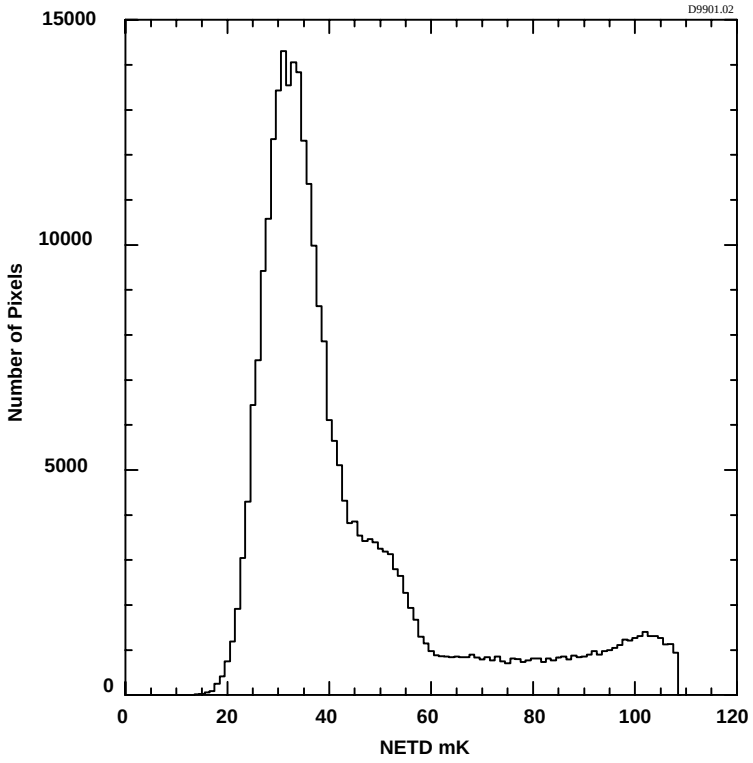


Figure 7. Estimate of FPACS NETD at 30 °C

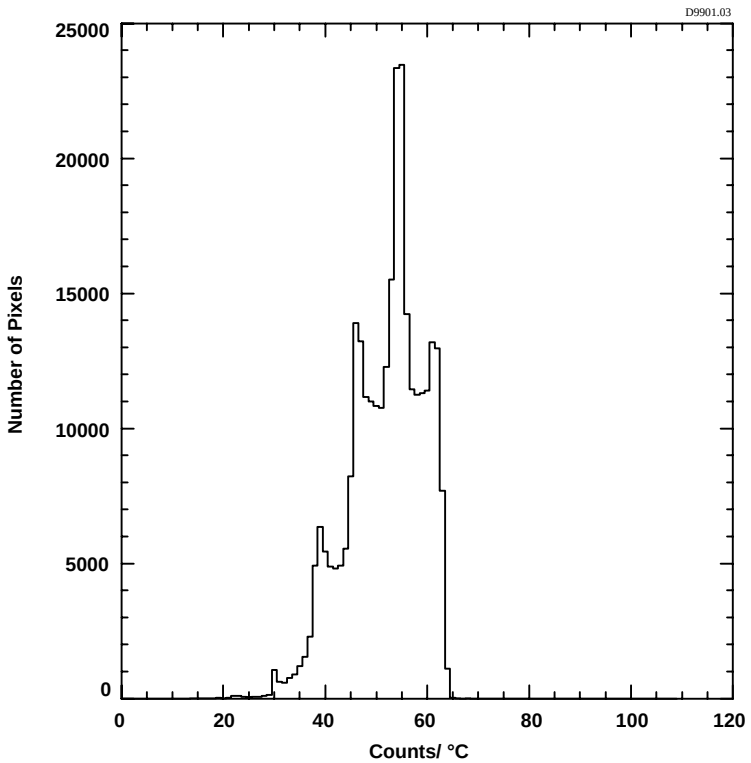


Figure 8. Approximation of FPACS Responsivity at 30 °C

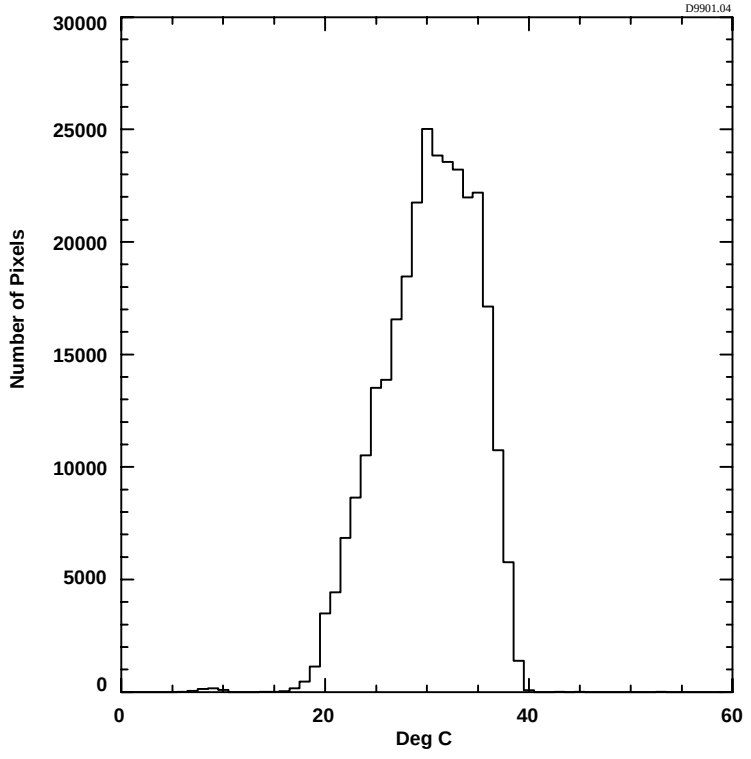


Figure 9. Approximation of FPACS Offset Bias at 30 °C

## 2.3 FPA PROCESSING ELECTRONICS

A functional block diagram of the FPAC interface electronics is provided in Fig. 10. Electrical signals generated by photon absorption are multiplexed in the Dewar and sent to an on-board interface module where signals are buffered and separated into two analog paths. The analog signals are converted to digital signals and paired. The ADSP 21020 Digital Signal Processor (DSP) has dual data busses and can perform multiply, add, and data move functions in a single clock cycle. The processor performs gain and level compensation on a pixel-by-pixel basis in real time. The DSP then applies a scale and offset to the raw pixel pair and stores resulting values in video memory. Images are produced in RS-170 video format by reading the image from video memory and converting the digital signals to analog format. Digital image data from the video memory is simultaneously made available on a digital port connected to a Windows-NT PC. In addition, a serial interface enables the host computer to communicate with the interface electronics. Commands are summarized as follows:

- control character annotation on video output,
- set the RGB values for video output lookup table,
- access gain & level adjustments for each pixel,
- set the detector integration time,
- adjust a global gain & level,
- define collection sequence in terms of X/Y dither and number of frames to collect,
- start, stop, and interrupt a collection sequence.

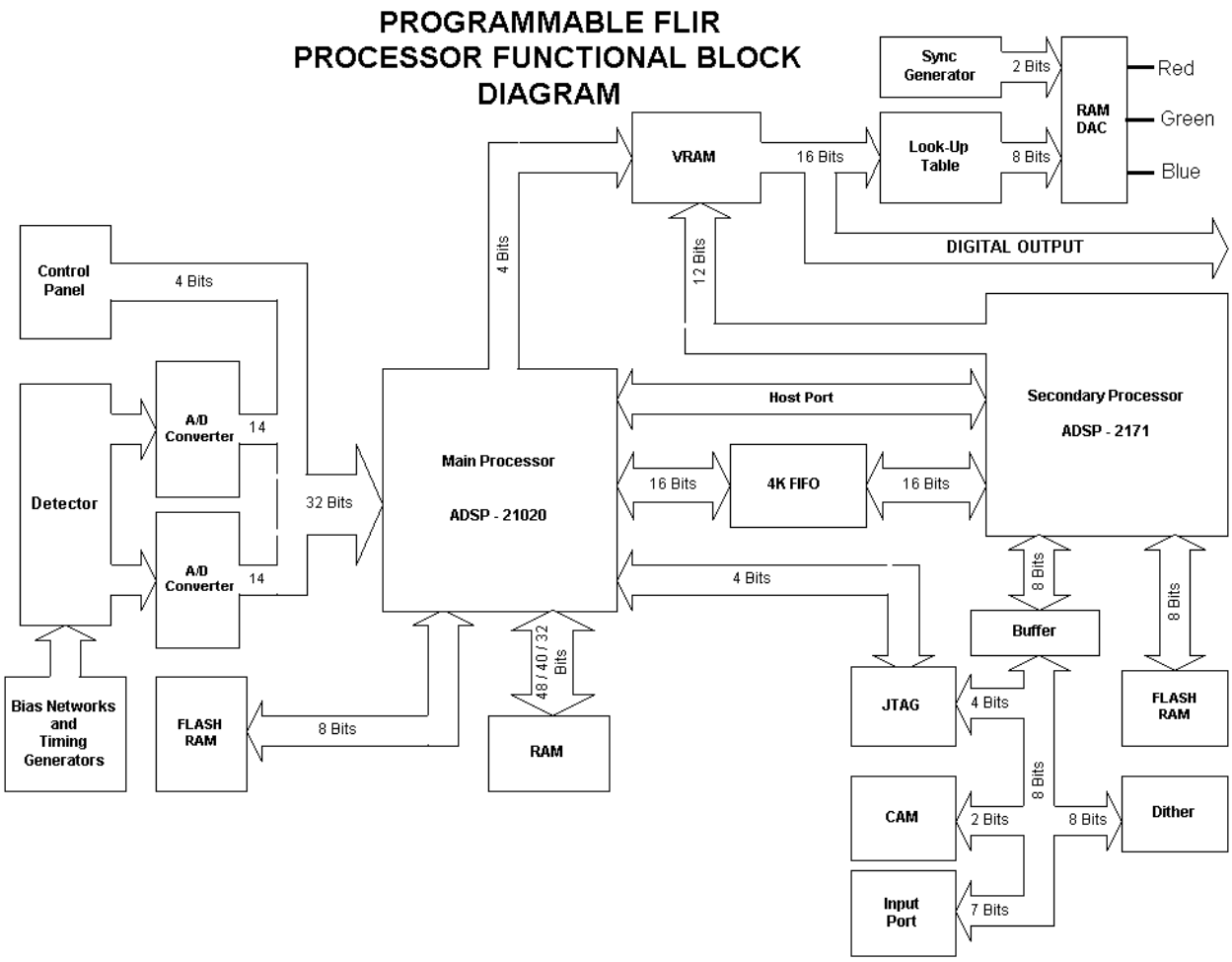


Figure 10. Sensor Interface Electronics Functional Block Diagram

## 2.4 DIGITAL RECORDING SYSTEM

Figure 11 depicts the scheme employed in the FPAC system to continuously record 12 bit digital data for approximately one hour. A commercially available PCI-type card "latches" digital data from the camera interface port and employs a Direct Memory Access (DMA) technique to stripe data over eight SCSI disks. Each disk records a separate bit. Software provided with the card uses the PC's DMA channels to transfer data from the camera interface to the SCSI interface over the PCI bus. The disk array appears as one large hard drive to Windows-NT PC.

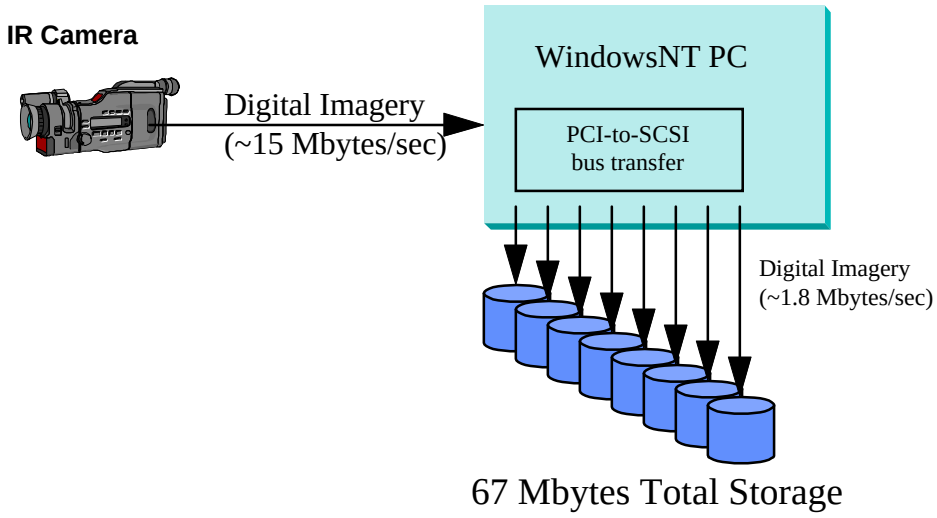


Figure 11. Parallel Disk Recording System

## 2.5 VIDEO TRACKER

The FPACS system includes a video tracker to provide continuous line-of-sight adjustments from a ground platform. The tracker is comprised of commercial-off-the-shelf components and utilizes the analog video generated by the camera interface electronics (see Fig. 12). Video is digitized to a precision of eight bits and used to drive an image correlation process. The operator uses the mouse to select a region in the digital scene that defines a track template. The template pixel pattern is compared with subsequent images utilizing the absolute difference between template pixels and new image pixels. The new position corresponds with the lowest sum of pixel differences. If the lowest absolute difference is sufficiently close to the average difference obtained over the entire search gate, then the new target position is deemed undetermined; and the system defaults to the position on which the search area is based. The new position is combined in a finite impulse response filter and used to predict the next search gate and target rate of change. The predicted rate is used to send commands to two motor controllers that in-turn activate stepper motors. The predicted position provides a basis to locate the search gate in the next image. Initial results indicate successful operation achieving a 12 Hz update rate. Development work on the tracker is continuing.

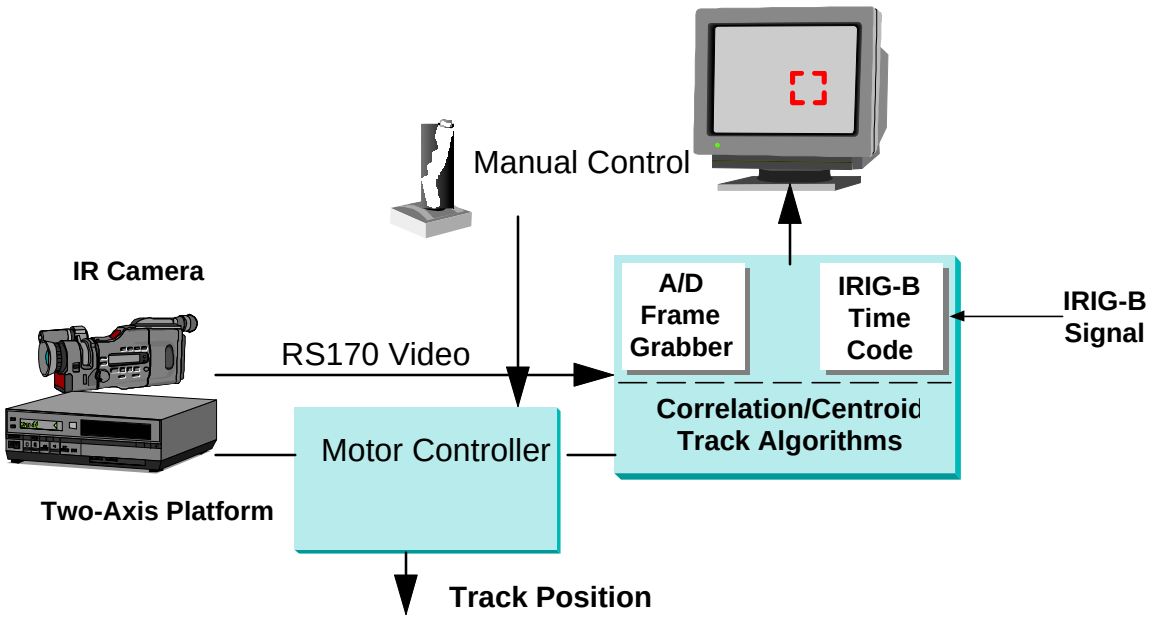


Figure 12. Video Tracking System

## 2.6 RADIOMETRIC CALIBRATION

Calibration is based on the fact that each detector element responds linearly to the average irradiance over the detector's photosensitive surface. There are two fundamental challenges in achieving an accurate calibration: 1) eliminating "stray" radiation, 2) calculating the irradiance over the detector surface from an estimate of blackbody temperature. Eliminating stray radiation is achieved by reducing the amount of thermal energy that strikes the detector from sources other than the object-of-interest. Stray radiation is primarily eliminated via good design practice. An anti-reflective lens coating, a re-imaging lens design with off-axis baffling, and proper geometric matching of the cold shield are all employed in the FPAC system.

Radiance from a calibration surface is indirectly estimated by independent measurements of temperature, emissivity, and the assumption that the calibration surface is both lambertian and obeys Planck's spectral distribution. In practice, these estimates often contain errors and can lead to inaccurate estimates of the object's true radiance, particularly when deployed to a remote site in an uncontrolled environment. The exitant radiance predicted from the calibration surface is attenuated by the atmosphere and sensor spectral response. For an extended calibration source, the spectral radiant intensity corresponding to a single pixel can be expressed as,

$$I = \varepsilon L_{BB}(\lambda, T_{BB}) R\alpha_h R\alpha_v, \qquad \text{(Eq. 1)}$$

where,

$I$ = Radiant Intensity

$\varepsilon$ = Surface emissivity

$L_{BB}(\lambda, T_{BB})$ = Planck's blackbody spectral radiance function

$\lambda$ = Wavelength of blackbody radiation

$T_{BB}$ = Surface temperature

$R$ = Range from camera to calibration surface

$\alpha_h$ = horizontal instantaneous field-of-view

$\alpha_v$ = vertical instantaneous field-of-view.

The solid angle from the calibration surface to the sensor's aperture is,

$$\Omega = \frac{\pi D^2}{4R^2}, \qquad \text{(Eq. 2)}$$

where D is the diameter of the entrance optics. By combining Equations 1 and 2, and integrating over the sensor's spectral response curve, the irradiance at the detector can be described by,

$$E = \frac{\pi \varepsilon D^2 R\alpha_h R\alpha_v}{4R^2 f\alpha_h f\alpha_v} \int_{\lambda 2}^{\lambda 1} L_{BB}(\lambda, T_{BB}) R(\lambda) \tau(\lambda) d\lambda \qquad \text{(Eq. 3)}$$

where,

$E$ = Irradiance at the detector

$f$ = Optics focal length

$R(\lambda)$ = Sensor normalized response (including optics transmission)

$\tau(\lambda)$ = Atmospheric transmission function.

Simplifying, Equation 3 results in,

$$E = \frac{\pi \varepsilon}{4F^2} \int_{\lambda 2}^{\lambda 1} L_{BB}(\lambda, T_{BB}) R(\lambda) \tau(\lambda) d\lambda \qquad \text{(Eq. 4)}$$

where F is the optics F-number. A typical calibration process involves imaging several calibration surfaces, measuring the corresponding surface temperatures, and predicting E for each surface radiance. Implementation of Equation 4 requires an estimate of both $\tau(\lambda)$ and $R(\lambda)$. Atmospheric transmission is typically approximated using the LOWTRAN model and the sensor response function is determined through empirical measurement. E is then linearly related to the average pixel value contained in the portion of the digital image corresponding with the calibration surface. Least Squares Regression is typically used to approximate this linear relationship.

Predicting the equivalent blackbody temperature of an unknown object implements the reverse of the calibration process. A pixel value is used in the calibration equation to calculate E. E is then related to a blackbody temperature value via a lookup table. This process compensates

for the radiant energy attenuated by the sensor's spectral response function and/or the atmospheric transmission. A "lookup" table provides a fast and accurate mechanism to determine an equivalent blackbody temperature.

## 2.7 SPATIAL CALIBRATION

In addition to radiometric calibration, FPACS also includes the ability to spatially calibrate pixels, provided two images have been collected according to the stereo geometry illustrated in Fig. 13. Spatial calibration derives the three dimensional position of a particular point by exploiting the parallax associated with the point. In the image obtained at camera station 1, point T appears to be positioned at point $T_1$. In a similar fashion, point T in the image obtained at camera position two appears to be at position $T_2$. This relationship is described by the collinearity equations,

$$x_i = f\frac{m_{11}(X_o - X_c) + m_{12}(Y_o - Y_c) + m_{13}(Z_o - Z_c)}{m_{31}(X_o - X_c) + m_{32}(Y_o - Y_c) + m_{33}(Z_o - Z_c)}$$

$$y_i = f\frac{m_{21}(X_o - X_c) + m_{22}(Y_o - Y_c) + m_{23}(Z_o - Z_c)}{m_{31}(X_o - X_c) + m_{32}(Y_o - Y_c) + m_{33}(Z_o - Z_c)} \qquad \text{(Eq 5)}$$

where,

| | |
|---|---|
| $x_i, y_i$ | = coordinates of the point at the focal plane of the camera, |
| $X_c, Y_c, Z_c$ | = position of the camera, |
| $X_o, Y_o, Z_o$ | = position of the point, |
| f | = focal length of camera optics, |
| $m_{ij}$ | = direction cosines between object-space and camera space. |

The collinearity equations are derived using a "pin-hole" camera model wherein a point on the ground, the camera aperture, and the corresponding point in the camera's focal plane lie along a straight line. The $m_{ij}$ coefficient in Eq. 5 and the camera position are typically established using an interactive least square technique. Points having known coordinates (ground control points) along with the associated image coordinates are used to establish a series of equations of the form of Eq. 5. Each ground control point yields a pair of expressions according to Eq. 5 for each image.

Images that have been spatially calibrated can be viewed in stereo using the FPACS Windows NT workstation. The operator perceives depth by isolating the image presented to each eye. Several different techniques are commercially available to achieve this image-to-eye isolation. The simplest and least expensive method is know as an anaglyph, which utilizes color to achieve stereo perception. The left image is stored in the red channel of an RGB image and the right image is stored in the blue channel. Glasses with a red lens and blue lens provide the image-to-eye isolation. Another technique is based on a pair of liquid crystal glasses. The glasses use liquid crystal lenses over each eye that are shuttered synchronously with the display of the left/right image. This technique requires a video card and monitor capable of operating at

a higher vertical refresh rate. The result is that objects appear to possess depth along a line perpendicular to the display surface.

Spatial calibration enables the FPAC system to equate the left/right pixel location with a specific three dimensional coordinate. In a single image, there are an infinite number of points that yield the same coordinate at the focal plane. From the perspective of Camera Station 1 in Fig. 12, points T and $T_1$ appear to be at the same position. The same is true of points T and $T_2$ from the perspective of Camera Station 2. Determining the three dimensional coordinate of point T involves an interative process in which Eq. 5 is evaluated separately for both The point at which both solutions agree is point T. In practice, the operator "floats" a cursor in apparent three dimensional space to the point to be measured (point T). The system actually draws two cursors, one at position $T_1$ in the image collected at Camera Station 1, and the other cursor at position $T_2$ in the image acquired at Camera Station 2.

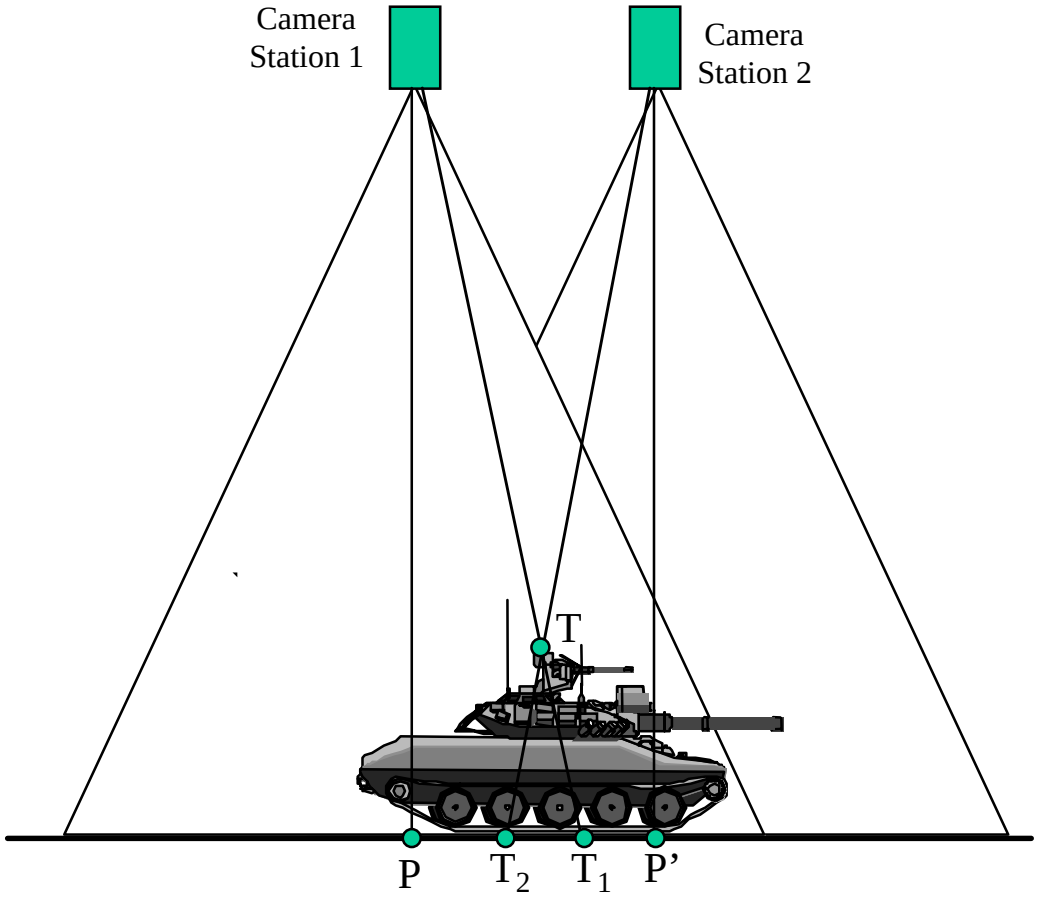


Figure 13. Stereo Image Collection Geometry

## 3.0 SUMMARY & CONCLUSIONS

The FPAC system is designed to provide state-of-the-art resolution and radiometric accuracy in a 3-5 micron infrared camera system. The system incorporates a five-degree FOV lens, with a motorized focus and three-position filter wheel. The filter wheel provides a peltier calibration surface and one percent transmission filter for use in imaging high-temperature objects. An intermediate focal point in the lens is combined with internal baffling to block off-axis radiation from reaching the detector. In addition, temperature sensors mounted within the lens assembly help monitor changes in environmental conditions. The detector is comprised of a 640 by 512 InSb array with an image dithering mechanism. The dithering mechanism consists of a germanium window mounted in a piezo-electric frame in front of the dewar which provides a one-half pixel shift of the image with respect the FPA. The resulting image consists of 1280 by 1024 pixels and is output to a precision of 12 bits every 0.13 seconds (7.5 Hz frames per second). A parallel disk recording system captures this digital data for up to one hour of continuous operation. Data are post-processed to achieve both radiometric and spatial calibration. Radiometric calibration is achieved by processing imagery of calibration blackbodies. Spatial calibration is achieved by photogrammetric processing of a stereo image pair and known control points.

FPAC system development began in July, 1997 and is scheduled to be completed in July 1999. One of the primary development issues involved coordination among different subsystem manufacturers. The initial detector array was rejected due to a large cluster of pixel outages. The dither device, which is an active optical element, involved close coordination with both the lens and detector manufacturer. All of these factors have combined to require more time than originally projected, although system delivery is still anticipated to be on time. Initial analysis of data suggests good sensitivity and resolution. Data also suggest that gain and level compensation are keys factors in establishing radiometric accuracy, with the latter being the most significant error source. Remaining tasks involve characterizing system performance, particularly with respect to radiometric accuracy. Projected unit cost of the system is approximately $250 K.